Synthesis of ZnO Particles in a Quench-Cooled Flame Reactor

Jens P. Hansen, Joakim R. Jensen, Hans Livbjerg, and Tue Johannessen
Interdisciplinary Research Center for Catalysis (ICAT), Dept. of Chemical Engineering, Technical University of Denmark, DK-2800 Lyngby, Denmark

The quench cooling of a flame by injection of cold air was studied in a flame reactor for the formation of ZnO particles in a premixed flame with a precursor jet. A rapid temperature drop downstream from the temperature peak is advantageous for the attainment of a large specific surface area. Computational fluid dynamics simulations were used to design a quench ring with nozzles directed slightly upward and at a small tangential angle from the direct line to the center. This novel design avoids distortion of the flow pattern below the quenching plane and effectively cools the flame immediately above. At the highest tested production rate, the specific surface area of the ZnO particles increases from 20 to 60 m^2/g when quenching is employed. The particles are characterized by BET surface area measurements,TEM images, and the size distributions of particle aggregates are measured by a scanning mobility particle sizer.

Introduction

The flame-aerosol synthesis of small particles with a high specific surface area is used in the materials industry for the manufacture of several important products. The flame-synthesis route also appears promising in the development of new materials, for example, catalysts and membranes, with unique properties (Pratsinis, 1998).

A flame-aerosol process is initiated by the combustion of volatile precursor vapors to form product molecules in a state of high supersaturation. The product molecules nucleate to form a myriad of small particles, which subsequently grow by coagulation due to interparticle collisions. In the individual aggregate particles, formed by coagulation of smaller particles, these start fusing together to form a compact shape by the surface-tension-driven process called sintering or coalescence. It has been recognized for some time that the ratio of the two independent rates, that is, that of coagulation to that of sintering, is the principal factor determining the particle morphology and the specific particle surface area in many flame-aerosol processes (Johannessen et al., 2000; Pratsinis, 1998; Wu et al., 1993; Windeler et al., 1997; Kruis et al., 1993). A low ratio value, that is, rapid sintering, yields a low surface area and singular compact particles. A high value, that is, slow sintering, yields high surface areas and particles shaped as dendritic aggregates of numerous smaller primary particles.

Sintering of nanoparticles may occur by any of several mechanisms (Frenkel, 1945; Kingerey, 1978; Lehtinen, 1997; Zachariah and Carrier, 1999), but the sintering theory for nanoparticles is as yet poorly developed. However, temperature is the most important factor affecting the sintering rate (Johannessen et al., 2000; Wu et al., 1993). To produce high surface-area materials, the height and duration of the flame temperature peak must be limited to that necessary for the complete decomposition of the precursor and the generation of the desired atomic structure of the particles. Thermal treatment in excess hereof only accelerates the degradation of the specific surface area by sintering.

Several types of flame-reactors have been employed in previous studies of flame aerosol processes, that is, diffusion flames (Johannessen et al., 2000), premixed flames (Jensen et al., 2000), premixed flames with a free precursor jet (Wu et al., 1993; Lehtinen, 1997; Johannessen, 1999). Downstream from the temperature peak, these flames are normally cooled by emitting radiation and by the free convective intermixing of the surrounding cold air. These mechanisms yield a slow and poorly controllable cooling rate and keeps the particles at the high temperature for an unnecessarily long time, which is incompatible with the desire to avoid excessive thermal

Correspondence concerning this article should be addressed to T. Johannessen.

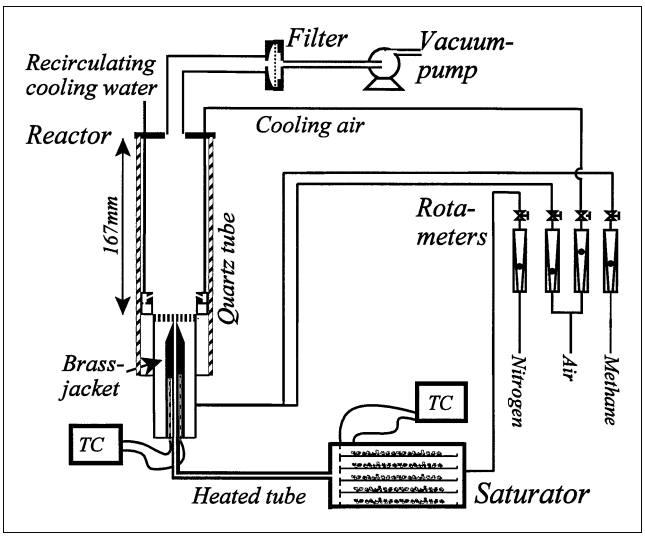

Figure 1. Experimental setup.

TC = temperature controller.

treatment. In this study, we investigate the possible improvement by quench cooling such flames to reduce the sintering rate and increase the specific surface area of the effluent particles.

Experimental Setup

The laboratory apparatus is shown on Figure 1. The premixed flame with a central precursor jet is a modification of the burner used by Wu et al. (1993) and Windeler et al. (1997). Premixed methane and air react in a flat zone just above the arrestor plate. The arrestor is circular, 40 mm in diameter, 5 mm thick, and gives an even distribution of the methane/air mixture. The jet outlet in the center of the arrestor is 1.27 mm in inner diameter. The jet consists of nitrogen mixed with vapors of the precursor, zinc acetylacetonate ($Zn(acac)_2$).

The saturator, in the design of Jensen et al. (2000), is a small thermostated steel box with five 85-cm^2 stainless-steel trays with layers of powdered $Zn(acac)_2$. On passing the saturator, the nitrogen stream of 0.23 L/min becomes saturated with precursor vapors. The concentration of the precursor in the nitrogen carrier gas is determined by the temperature of the saturator. To prevent condensation of the precursor in the transport tube, the temperature of the tube from the saturator to the burner is kept approximately 20°C higher than the saturator temperature.

An important modification of the original burner is the quench ring above the arrestor used for rapid cooling of the flame product gasses. The flame reactor is kept in a quartz-tube shield, which is open only at the top. The entire setup is placed in a fume hood. The quench ring is cooled internally with liquid water to avoid overheating the metal and the cooling air. The cooling water is preheated to 50°C to prevent condensation of water from the combustion gas on the cooled surfaces in the reactor.

All flow rates are measured by calibrated rotameters. In all experiments, the flow rates of methane and air to the burner are held at 0.62 and 9.87 L/min, respectively. Furthermore, the nozzle outlets of the quench ring were fixed at 17 mm above the arrestor plate, as shown on Figure 2. The product gas is drawn through a filter with 1.0-μm pore size by a vacuum pump to collect the particles.

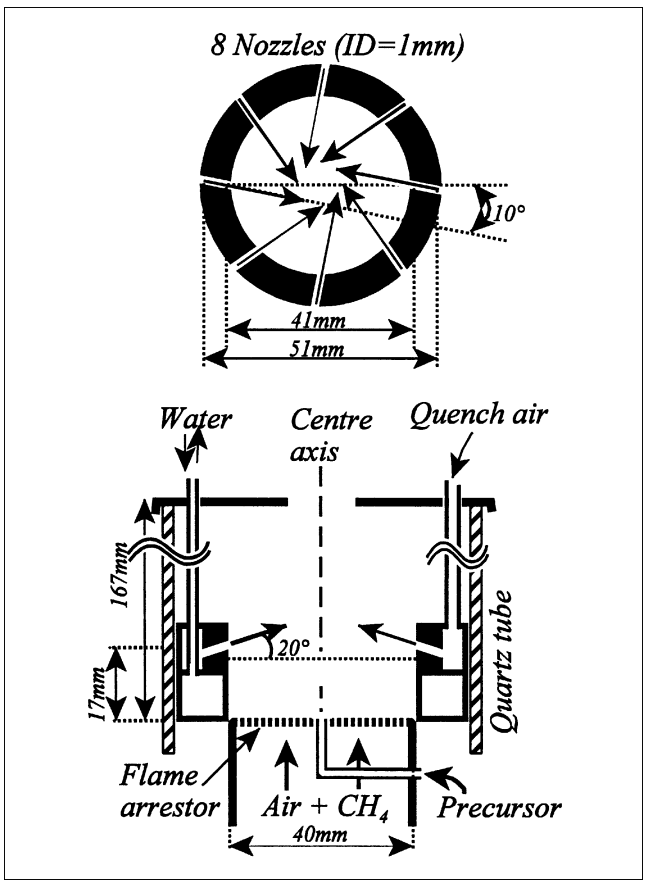

Figure 2. Flame reactor and quenching device.

Note that the total height is not drawn to scale; the nozzles are pointing upward with an angle of 20°. Top: top view of the stainless steel block in the quench ring; each nozzle has an angular offset of 10° relative to an imaginary line through the center axis.

Design of the Quench Ring

For the initial experiments, the quench ring was designed with horizontal nozzles directed toward the center axis (Johannessen, 1999). This design yields serious distortions of the flame due to vortex formation and downward-directed flow below the quenching zone. In worst cases, the cooling air extinguishes the flame. No improvement of the specific particle surface area were obtained with this quench design.

Computational fluid dynamic (CFD) simulations were subsequently used to improve the design of the quench ring. Although the quench ring has a finite number of nozzles, the simulation has been simplified by assuming rotational symmetry around the center axis of the reactor. By this approximation, the nozzles are simulated as a thin slit with an effective area equal to the area of all the circular jets.

As a first attempt to stabilize the flow, the nozzles were tilted upwards, directed at the center axis, but simulations show that a stable flow is only obtained by imposing a tan-

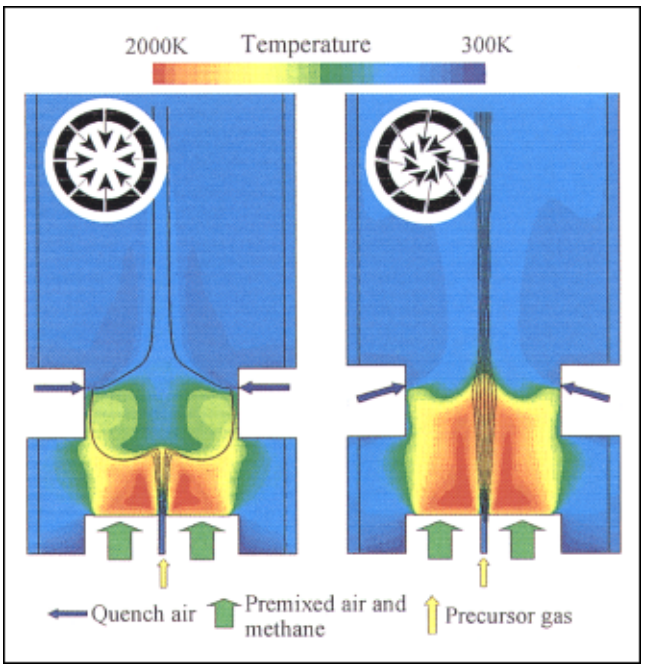

Figure 3. Predicted temperature fields (computational fluid dynamics) for the initial quenching system (left) and the proposed design (right).

The nozzles in the novel quench ring are oriented slightly upwards with a tangential component of 10°. The black lines represent average particle paths of massless particles following the mean flow field of gasses. The particle trajectory depends on the initial position of the particle in the precursor jet. The new design eliminates any distortion of the temperature and flow field below the quenching point.

gential velocity component in addition to the axial component.

The predicted temperature profiles and average particle trajectories are shown on Figure 3 for both the initial and final quenching design. For the initial design (Figure 3, left), the distortion of the flame below the quenching point causes the particle trajectories to diverge and follow poorly shaped paths with no steep temperature gradients. With the improved design (Figure 3, right), the particle trajectories are only slightly perturbed and they all traverse a very steep and well-defined temperature drop located just above the quenching zone. It is very clear from Figure 3 that a drastic improvement in the quenching efficiency is obtained by these minute changes in the quench configuration.

The flow simulations are made with the commercial CFD-code FLUENT. Johannessen (1999) and Johannessen et al. (2000) provide further details.

Characterization of the Particles

The specific surface area, S_A, is measured by multipoint nitrogen adsorption (Gemini 2360, Micromeritics) at 77 K using the BET equation. Assuming spherical particles, one can calculate a BET equivalent primary particle size, D_{BET}, from

$$D_{\mathrm{BET}} = \frac{6}{\rho_p S_A}, \qquad (1)$$

where ρ_P is the solid density.

Grids for transmission electron microscopy (TEM) where prepared in a suspension of a small amount of particles in liquid ethanol. The suspension was treated with ultrasound to deagglomerate the particles.

The size distributions of particles/aggregates were measured with a scanning mobility particle sizer (SMPS) system consisting of a differential mobility analyzer (DMA 3071A, TSI) and a condensational particle counter (CPC 3022, TSI). A gas ejector sampler withdraws a small sample flow of product gas through a capillary tube and dilutes it prior to analysis (Nielsen and Livbjerg, 2000). This sampling technique has the advantage of a low residence time (< 20ms) of the hot and concentrated aerosol in the capillary tube, and the subsequent, immediate cooling and dilution of the sample stream effectively quenches further particle sintering and strongly reduces the coagulation rate of particles.

Results and Discussion

Experiments verify that the nozzles in the quench ring can operate as low as 17 mm above the arrestor without making any visibly distorting of the flame. The temperature profiles have been measured along the vertical-symmetry axis (the jet axis) with a Pt/PtRh thermocouple with a welding point of the free 0.2-mm thermowires inserted into the selected location of the flame. The temperatures shown are not corrected for radiation loss, so the actual temperature level is slightly higher. The magnitude of the correction depends on both the temperature and the gas velocity at the measuring point. A high temperature and a low velocity yield the highest radiation correction. Therefore, the two cases with and without nitrogen jet are not directly comparable in terms of the level of the peak temperature. Even so, the uncorrected profiles are excellent qualitative measures of the temperature variation within the flame. Figure 4 shows temperature profiles without nitrogen flow in the precursor jet. Without quenching ($Q = 0$ L/min), the measured temperature drops slowly downstream from the premixed reaction zone. With quench-

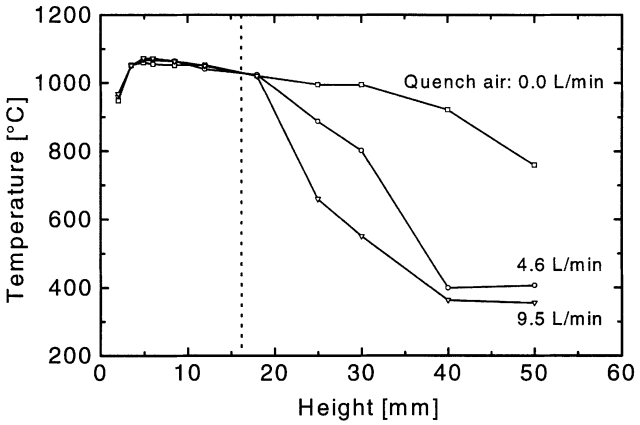

Figure 4. Temperature profiles along the vertical jet axis without jet flow.

The outlets of the quench nozzles were positioned 17 mm above the arrestor; the flow of nitrogen in the jet is 0 L/min.

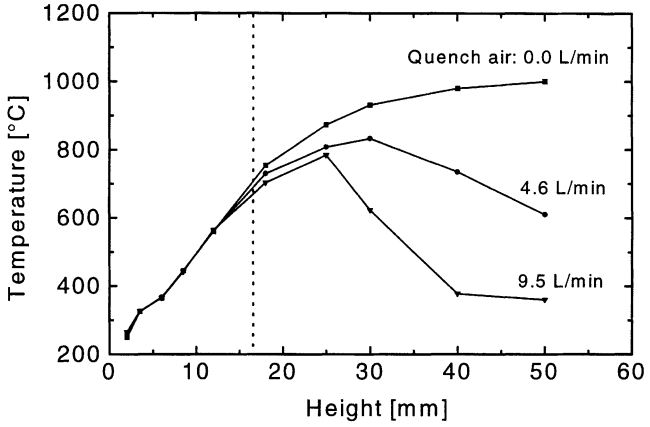

Figure 5. Temperature profiles along the vertical jet axis with jet flow.

The outlets of the quench-nozzles are positioned 17 mm above the arrestor; the flow of nitrogen in the jet is 0.95 L/min.

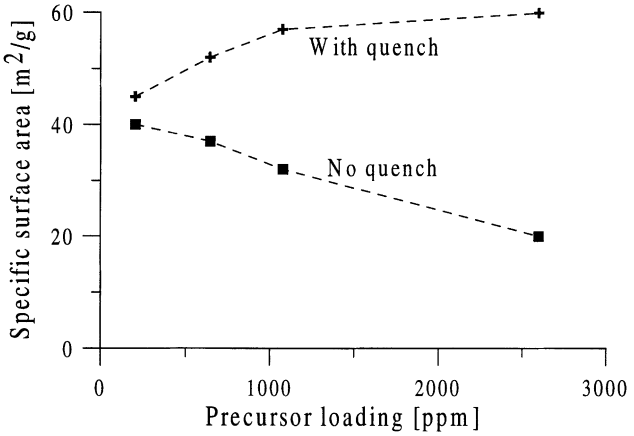

Figure 6. BET surface area of ZnO powder as a function of the temperature in the $Zn(acac)_2$-saturator.

The quench air flow is either 0 L/min or 9.5 L/min.

ing (Q = 4.6 or 9.5 L/min), the temperature starts decreasing rapidly from just above the quenching point, whereas the profiles remain unchanged below the quenching point. Figure 5 shows the corresponding temperature profile with 0.95 L/min of nitrogen in the precursor jet. The temperature of the jet is 150°C at the jet outlet in the center of the arrestor. For the profile without quenching, the temperature of the jet increases to approximately 1,000°C by mixing with the hot combustion gasses.

When quenching is applied, we again see an effective cooling of the jet above the quenching point and an unperturbed temperature below this point. Based on Figures 4 and 5, we can conclude that the design of the quench ring is indeed satisfactory. The selected direction of the quench nozzles evidently stabilizes the flow pattern without any disturbance below the quenching point. The tangential component of the quench jet flow must be chosen with care because a tangential flow that is too large yields a flow pattern where the jet "shoots" through the center of the quenching zone without being cooled. The measurements in Figure 5 clearly show that we have avoided this potential problem in the present design.

A series of experiments were carried out with four different temperature settings for the saturator thermostat. At each temperature, the precursor-vapor content in the effluent gas has been determined from the measured weight loss of the $Zn(acac)_2$ in the saturator, as shown in Table 1. For each of the four saturator temperatures, the burner is operated both with and without quenching, and the resulting specific surface area of the powders collected on filters is measured. The results are summarized in Figure 6. Without quenching, the specific surface area decreases when the precursor concentration in the feed increases. This agrees with the coagulation/sintering theory for flame synthesis of particles (Wu et al., 1993, Windeler et al., 1997). A high precursor concentration yields a high coagulation rate, and consequently a high mass per particle. If sintering is allowed to proceed uninterrupted by, for example, quenching, the particles with the largest mass obviously yield the smallest specific surface area, which is in agreement with Figure 6 for the runs without quench.

When the quench air is turned on, we see a substantial increase in the specific surface area, especially at high precursor concentrations. At $T_{sat} = 130$°C, which is equivalent to a 2600 ppm precursor, the specific surface area increases by a factor of 3. For the four experiments with quenching, the specific surface area increases moderately with increasing precursor concentration to become stabilized at approximately 60 m^2/g. We cannot explain this effect of the precursor concentration on the basis of the simple coagulation/sintering theory. If we extend the arguments for the runs without quench to include the interruption of sintering as an effect of quenching, the theory at best predicts a constant specific surface area, independent of the precursor concentration. It is possible, though, that the precursor decomposition/combustion is not instantaneous, as assumed by the simple theory. The kinetics of this reaction, which is poorly known, may delay the liberation of solid particles below the

Table 1 BET-equivalent Primary-Particle Diameter (D_{BET}) and Mean Surface-Area Diameter ($D_{a,sa}$) from SMSP Data

Saturator Temp.	ppm $Zn(acac)_2$	With Quenching (nm)		No Quenching (nm)	
		D_{BET} (eq. 1)	$D_{a,\,sa}$ (eq. 3)	D_{BET} (eq. 1)	$D_{a,\,sa}$ (eq. 3)
100°C	203	24	26	26	27
110°C	647	22	43	29	36
120°C	1,079	19	60	33	58
130°C	2,601	18	—	52	—

quenching point to bring about the observed increase in surface area. A slow decomposition rate was actually indicated by some experiments with a much higher jet flow, for which the collected particles were discolored, presumably due to an incomplete acetonate decomposition. However, clearly the heterogeneous environment of the flame does not lend itself easily to simple theories, and the flame processes is currently being analyzed by computational fluid particle dynamics to examine in more detail the interactions between the different flame processes.

Values of the BET-equivalent primary particle diameter, D_{BET}, calculated by Eq. 1, are shown in Table 1. Without quench, the diameter increases from 26 nm to 52 nm, when the precursor concentration is increased from its lowest to its highest value. With quench, the diameter decreases from 24 nm to 18 nm during the same variation of the precursor concentration. TEM images for a saturator temperature of 120°C are shown in Figure 7. The particles are oblong and hexagonal in structure, and diffraction images show that the particles are crystalline. The hexagonal wurtzite structure of ZnO is stable at ambient temperature and pressure (Kunnert, 1981). The degree of agglomeration in the gas phase cannot be assessed from the TEM-images, since the observed agglomerates may have been formed during the deposition on the filter or in the liquid phase during the preparation of the grids.

Figure 8 shows the normalized size distributions of aggregates. No attempt has been made to correct for the variation of the dilution ratio in the ejector from one run to another, since we wish to compare only the shapes and mean sizes of the distributions. Hence, in Figure 8 all distributions are scaled to yield a value of 100 as the maximum value.

For spherical and nonagglomerated particles, the number size distribution, n, from the SMPS measurements can be transformed to a surface-area distribution (Friedlander, 1977):

$$n_s(\log D_a) = \pi D_a^2 n(\log D_a). \tag{2}$$

From the total surface area, a mean surface-area diameter, $D_{a,sa}$, can be calculated:

$$\overline{D_{a,sa}{}^2}\pi = \frac{1}{N}\int_{-\infty}^{\infty} n_s(\log D_a)\, d\log D_a. \tag{3}$$

For particles, which are aggregates of several primary particles, $D_{a,sa}$ is a measure of the aggregate size.

Table 1 compares D_{BET} and $D_{a,sa}$ for all runs. The two diameters are almost identical at low precursor concentration, both with and without quenching, which indicates that the particles are singular and nonagglomerated. The difference between the two diameters increases when the temperature in the saturator increases, which proves that the particles become aggregates of smaller primary particles at higher precursor concentrations. The ratio of $D_{a,sa}$ to D_{BET} increases on quenching, and this effect of quenching is particularly significant at the high precursor concentration. Thus, the quenching yields smaller, but more primary particles per aggregate than without quenching, especially at high precursor concentration. The resulting effective aggregate size, $D_{a,sa}$, is rather independent of quenching, as seen from the values in Table 1 and the distributions in Figure 8.

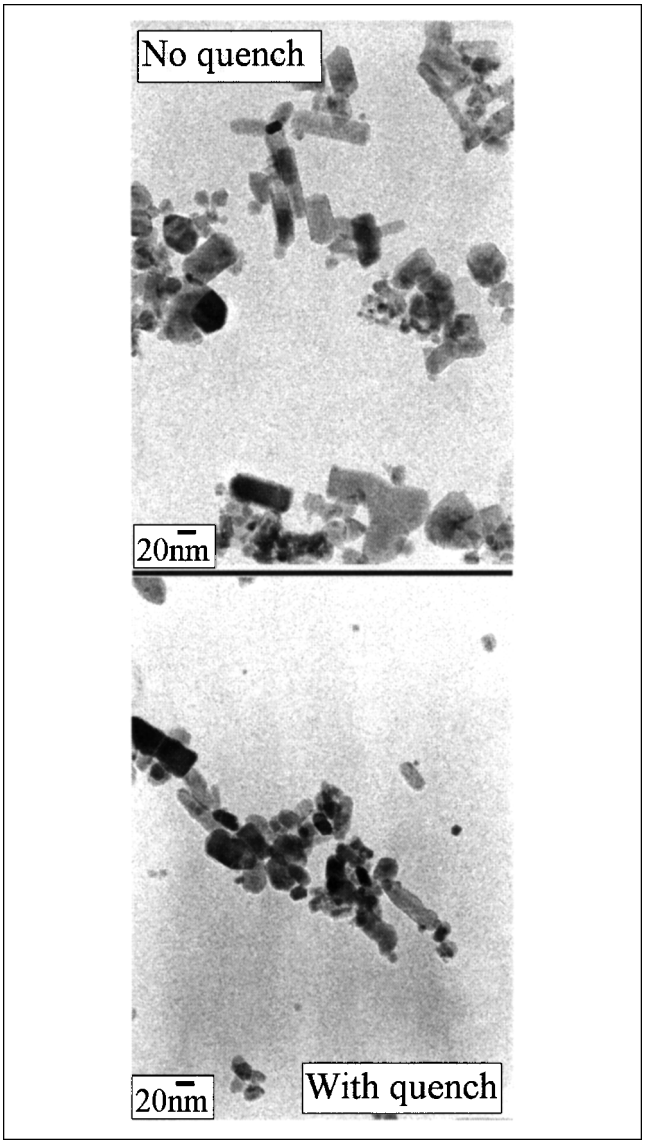

Figure 7. TEM images of particles from experiments with a saturator temperature of 120°C; without (top) and with (bottom) quenching air.

Conclusion

Based on CFD simulations, we have designed a novel quenching device, which has proved useful in controlling the coalescence of aggregate particles in a flame reactor. By directing the quench nozzles upwards at an angle of 20° with a tangential component relative to the center axis, we obtained a well-defined, rapid cooling of the combustion gasses and the particle jet. When the flame is quenched, the temperature drops sharply by up to 600°C above the quench-zone, but is virtually unchanged below the quench zone. Because the cooling air has very little impact on the flow and temperature conditions below the quench zone, it is possible to op-

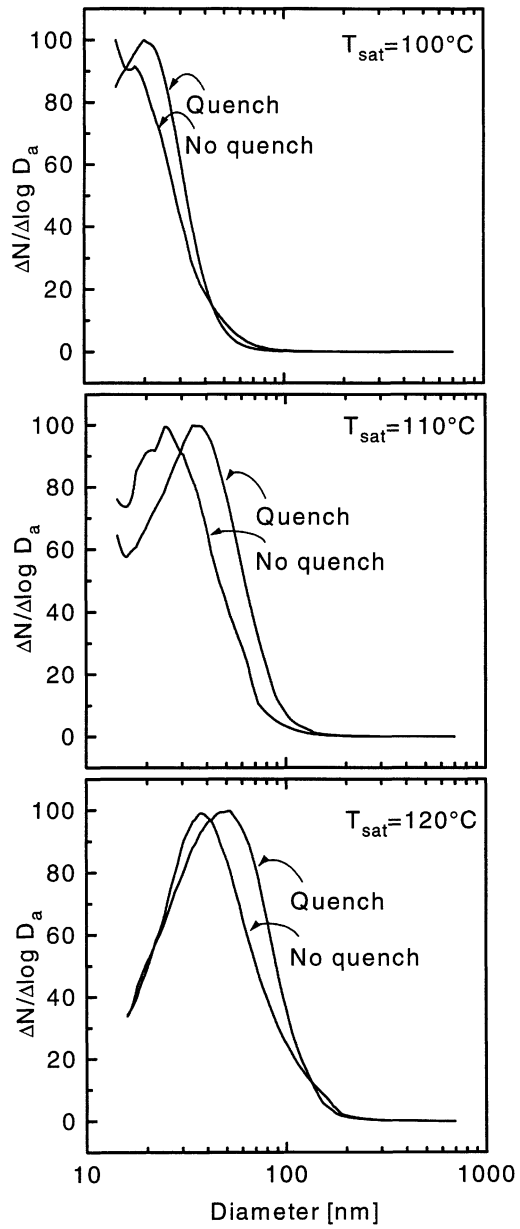

Figure 8. Normalized SMPS particle-size distributions.

erate the quench nozzles as low as 17 mm above the arrestor plate. Consequently, the rate of coalescence of particles can be controlled during a very early stage of the particle formation process.

A significant increase in specific surface area of the produced ZnO particles is observed as a result of quenching. The effect of quenching is particularly significant at high precursor concentrations. The specific surface area increases by a factor of 3, from 20 m^2/g to 60 m^2/g, for the experiment at 130°C in the saturator, but the effect is less at lower precursor concentrations. Since the results are best at high particle mass loadings, the quenching process is particularly promising for industrial processes where a high production rate is wanted.

The decrease of particle sizes is confirmed by the TEM images. However, a direct comparison between the BET equivalent size and the size based on the TEM images is difficult since the particles are nonspherical, hexagonal structures that are significantly different in size.

SMPS-measurements show that both quenching and increasing the precursor concentration shift the size distribution toward larger aggregates. A comparison of the mean aggregate diameter from the SMPS measurements with the BET equivalent diameter shows that the particles are non-agglomerated at the reactor outlet at low precursor concentrations, both with and without quenching. At higher precursor concentrations, that is, for saturation temperatures of 110°C, 120°C, and 130°C, the particles are evidently aggregates/agglomerates of several small primary particles. The number of primary particles per aggregate increases with increasing precursor concentration.

Quenching the flame process by cold air has proved to be an effective method for increasing the specific surface area, even at high precursor concentrations. The perspectives for further improvements of particle characteristics by optimizing process condition are promising. However, the design of the quench system must always be delicately balanced to avoid the complete destruction of the flow pattern below the quench point.

Acknowledgments

This work was funded by the Danish Research Councils.

Literature Cited

Frenkel, J., "Viscous Flow of Crystalline Bodies under the Action of Surface Tension," *J. phys.*, **9**, 385 (1945).
Friedlander, S. K., *Smoke, Dust and Haze*, Wiley, New York (1977).
Jensen, J. R., T. Johannessen, S. Wedel, and H. Livbjerg, "Preparation of ZnO/Al_2O_3 Particles in a Premixed Flame, *J. of Nanoparticle Res.,* **2**(4), 363 (2000).
Johannessen, T., *Synthesis of Nano-Particles in Flames*, PhD Thesis, Dept. of Chemical Engineering, Technical Univ. of Denmark, Lyngby (1999).
Johannessen, T., S. E. Pratsinis, and H. Livbjerg, "Computational Fluid-Particle Dynamic for the Flame Synthesis of Alumina Particles," *Chem. Eng. Sci.*, **55**, 177 (2000).
Kingerey, W. D., H. K. Bowen, and D. R. Uhlmann, *Introduction to Ceramics*, Wiley, New York (1978).
Kruis, F. E., K. A. Kusters, S. E. Pratsinis, and B. Scarlett, "A Simple Model for the Characteristics of Aggregate Particles Undergoing Coagulation and Sintering," *Aerosol Sci. Technol.*, **19**, 514(1993).
Kuhnert, R., R. Helbig, and K. Hümmer, *Phys. Status Solidi B*, **107**, 83 (1981).
Lehtinen, K. E., "Theoretical Studies on Aerosol Agglomeration Processes," PhD Thesis, VTT Technical Research Centre of Finland, Espoo, Finland (1997).
Nielsen, M. T. and H. Livbjerg, "A Gas Ejector Aerosol Sampler," (2000).
Pratsinis, S. E., "Flame Aerosol Synthesis of Ceramic Powders," *Prog. Energy Combust. Sci.,* **24**, 197 (1998).
Windeler, R. S., S. K. Fridlander, and K. E. Lehtinen, "Production of Nano-Meter-Sized Metal Oxide Particles in a Free Jet I: Experimental System and Results," *Aerosol Sci. Technol.*, **27**, (2), 174 (1997).
Wu, M. K., R. S. Windler, C. K. R. Steiner, T. Bors, and S. K. Friedlander, "Controlled Synthesis of Nanosized Particles by Aerosol Processes," *Aerosol Sci. Technol.*, **19**, 527 (1993).
Zachariah, M. R., and M. J. Carrier, "Molecular Dynamics Computations of Gas-Phase Nanoparticle Sintering: A Comparison with Phenomenological Models," *J. Aerosol Sci.*, **30**, pp.1139 (1999).

Manuscript received Apr. 3, 2000, and revision received Sept. 20, 2000.